The Influence of Aluminum and Oxygen Additions on Intrinsic Structural Instabilities in Titanium-Molybdenum Alloys

Yufeng Zheng[1*], Talukder Alam[2], Rajarshi Banerjee[2], Dipankar Banerjee[3] and Hamish L. Fraser[1,]

[1]Center for the Accelerated Maturation of Materials and Department of Materials Science and Engineering, The Ohio State University, Columbus, OH 43212, USA.
[2]Materials Research Facility and Department of Materials Science and Engineering, University of North Texas, Denton, TX 76207, USA
[3]Department of Materials Engineering, Indian Institute of Science, Bengaluru, Karnataka 560012, India

* Corresponding author: Yufeng Zheng, zheng.510@osu.edu, CEMAS, The Ohio State University, 1305 Kinnear Rd., Suite 100, Columbus, OH 43212-1177, USA

Abstract

The influences of aluminum and oxygen additions on structural instabilities in the β phase of binary Ti-Mo alloys have been investigated, using conventional and aberration-corrected scanning/transmission electron microscopy and atom-probe tomography. An addition of 5wt%Al to the alloy Ti-18wt%Mo tends to decrease the stability of the 2/3<111> longitudinal phonon, compared with that of the phase O' formed by the {110}<1$\bar{1}$0> transverse phonon. Experiments have been performed to assess whether interstitial oxygen influences these phase instabilities by adding yttrium to getter the matrix oxygen. It has been found that oxygen is not a necessary alloying addition to form the O' phase.

Keywords: Titanium alloys; Phase transformations; High-resolution electron microscopy; ω Phase; O' phase

The investigation of instabilities in the β phase of metastable β titanium alloys has attracted considerable attention in recent years because of their influence on various aspects of microstructural evolution and mechanical behavior in this alloy class [1]. For example a transformation pathway to the equilibrium α phase using ω as a precursor can produce extremely refined dispersions of α in the alloy Ti-5553 [2] and has been exploited to produce very high strength levels in the alloy β-21S [3]. An alternative distinct nanodomain structure has been observed in metastable β alloys containing deliberate oxygen additions such as gum metal, by Yano *et al.* [4] and Tahara *et al.* [5]. The latter authors concluded that these nanodomains originated from a $\{110\}\langle 1\bar{1}0\rangle$ type transverse lattice modulation in the β phase [5] and that these nanodomains acted as barriers to transformation to orthorhombic martensite (α″). In a different study, Wang *et al.* [6] suggest that a Ti-Nb-Ta-Zr-O alloy (TNTZ-1.2O), alloy undergoes a 'strain glass transition' to 'martensitic nanodomains' [7, 8]. The 'martensitic nanodomains' in this study appear identical to those reported in [4, 5] based on similarities in diffraction. In all these studies, it has been suggested that the nanodomains form as a result of strain centers associated with oxygen atoms, with the implication [6-8] that oxygen additions are essential in the development of the unique properties of this class of alloys.

An alternative viewpoint for the formation of the $\{110\}\langle 1\bar{1}0\rangle$ nanodomains has been proposed in which the $\{110\}\langle 1\bar{1}0\rangle$ transverse wave is recognized to be a component of the martensitic transformation from β to the hexagonal α′ or the orthorhombic α″ martensite [9-11]. The martensite transformation occurs by the $\{112\}\langle 111\rangle$ shear that transforms the $\{110\}_\beta$ planes into the (0001) or (001) planes of α′ or α″, while a $\{110\}\langle 1\bar{1}0\rangle$ displacement wave leading to a shuffle on every alternate plane changes the stacking sequence of these planes, as proposed by Burgers in 1934 [12]. Thus it has been shown in [9] that when the $\{110\}\langle 1\bar{1}0\rangle$ shuffle occurs after the $\{112\}\langle 111\rangle$ shear (the Bain distortion) that transforms β to martensite, a domain structure related to these shuffles occurs within the martensite plates. However, if the shuffle precedes the shear, 12 variants of nanodomains can form completely coherently with the matrix since the parent cubic motif is retained by the shuffle. These domains have been imaged by ultra-high resolution high angle annular dark field imaging more recently in [10, 11] and designated as O′ (due to the orthorhombic

symmetry, Cmcm, of the nanodomains and to distinguish them from the equilibrium, ordered, orthorhombic O phase observed in Ti-Al-Nb alloys [13] and the ordered, orthorhombic phase, O″, in aged metastable β alloys [14]).

The objective of this paper is therefore two-fold. Firstly, the role of an α stabilizer on the relative stability of the O′ and ω phases is examined in two alloys, Ti-18Mo and Ti-18Mo-5Al (wt%). Secondly, a series of experiments is aimed at determining whether oxygen is a necessary alloying addition for the formation of the O′ phase. It is well known that oxygen will be present in essentially all alloys prepared from commercially available sponge. To produce an alloy where it would be known with certainty that oxygen is not contained in the alloy matrix, additions of yttrium have been made so that in the heat-treated condition, particles of Y_2O_3 would be formed because of the strong affinity of the rare earth element for oxygen (the thermodynamics of such Ti-rare earth alloys has been described previously [15]). Provided the concentration of the rare earth is such that there is an excess of yttrium in the matrix following formation of the oxide, the residual concentration of oxygen in the matrix will be at a vanishingly low value. Hence, yttrium was added into Ti-18Mo-5Al to essentially remove oxygen from the β matrix.

The Ti-18Mo alloy was the same as that used in a previous study [11]. The Ti-18Mo-5Al alloy used in current work was provided by the TIMET Corporation (Henderson, NV), and its composition measured by conventional wet chemistry, being Ti-17.29Mo-4.7Al-0.26O (wt%), of which the oxygen content is comparable to that in the Ti-18Mo. The as-received alloy (Ti-18Mo-5Al) was then annealed in a vacuum furnace at 1100°C for 96 hours and then furnace-cooled to room temperature, in order to promote its homogeneity. The bulk material was cut into 20mm×10mm×10mm pieces using electrical discharge machining (EDM) for further heat treatment in a tube furnace. Sectioned Ti-18Mo-5Al samples were β solutionized at 910°C, approximately 100°C higher than the calculated β transus temperature (assessed using Thermo-Calc), for 1 hour and quenched into water at room temperature. In order to further reduce the oxygen level in the β phase matrix, 0.9 gram pure yttrium (99.9%) was added to 22.8 gram the binary Ti-18Mo button (approximately 3.80wt%) and 31.1 gram the ternary Ti-18Mo-5Al button (approximately 2.81wt%) using

an arc-melter; in both of these yttrium containing alloys, there will be excess yttrium over that required to form Y_2O_3. These alloys, with the yttrium additions, were then β solutionized at 1000°C for 30 minutes and subsequently quenched into water. Thin foils for transmission electron microscopy (TEM) and high angle annular dark field- scanning transmission electron microscopy (HAADF-STEM) analysis were prepared using the Dual Beam Focused Ion Beam (DB-FIB) technique, using an FEI Helios Nanolab 600 system, and the resulting ion beam damage on the foil surfaces was minimized using low voltage Ar^+ ion milling in a Fischione Nanomill™ Model 1040. TEM dark-field images and diffraction patterns were recorded on a Philips CM200 transmission electron microscope operating at an accelerating voltage of 200kV. Line profiles from a number of TEM diffraction patterns were analyzed using ImageJ, and for each alloy a representative set of data for each diffraction pattern is presented. HAADF-STEM images were recorded using a probe-corrected FEI Titan3™ 80-300 S/TEM operated at 300kV, using a convergence semi-angle of 12 mrad and a collection semi-angle of 44 mrad, with an incident beam dwell-time of 4µs/px and a beam current of ≈ 90pA. X-ray energy dispersive spectrometry (XEDS) analyses were performed in an aberration-corrected (S)TEM (FEI Titan3™ G2 60-300 S/TEM at 300kV), equipped with a SuperX (FEI) four-quadrant silicon drift detector. Needle shape samples were prepared using the FEI Nova 200 NanoLab and analyzed in Cameca 3000X HR local electrode atom probe (LEAP) system, using the voltage mode at a temperature of 60K, with an evaporation rate 0.5-0.7% and a voltage pulse fraction of 20% of the steady-state applied voltage, for 3D atom probe (3DAP) tomography. 3D reconstruction and chemical composition measurement were done using IVAS® 3.6.8 software.

The influence of Al additions on the relative stability of the metastable phases (O' and ω) in Ti-18Mo is first assessed. A selected area diffraction (SAD) pattern recorded from a sample of as-quenched Ti-18Mo-5Al with the electron beam parallel to a $<110>_\beta$ zone axis is shown in Fig. 1 (a). In this diffraction pattern, ω reflections are observed at $1/3\{112\}_\beta$ and $2/3\{112\}_\beta$ locations and highlighted by white circles in Fig. 1(a). Besides reflections arising from the ω phase, another set of extra reflections may be observed at $1/2\{112\}_\beta$ locations, an example being indicated by the white arrow. These reflections may be

attributed to the presence of the O' phase based on previously published results [10, 11]. A $<100>_{\beta}$ zone axis diffraction pattern and corresponding dark field image formed from an O' reflection at $1/2\{310\}_{\beta}$ in solution-treated and quenched Ti-18Mo-5Al are shown in Fig. 1(b). From the image, it is evident that the nano-scale O' phase particles are homogeneously distributed in the β matrix, and is similar to the microstructures reported in quenched Ti-26Nb-2Zr (at%) [10] and Ti-18Mo (wt%) [11]. A comparison of the HAADF images exhibited by the O' and ω phases are presented in Fig. 1(c and d). It is evident that both alloys, Ti-18Mo and Ti-18Mo-5Al, in the solution-treated and quenched conditions contain both O' and ω phases.

Any possible influence of Al on the relative stability of the two phases may be assessed from a comparison of the relative intensities of the reflections from these phases in the presence and absence of Al additions. Therefore, line profiles in the diffraction patterns, plotted from the forward scattered beam (000) to one of $\{112\}_{\beta}$ reflections (indicated by the dashed white line), are shown in Fig. 2(a) from SADs obtained from these two alloys. For the binary alloy, the diffracted intensity from the ω phase is relatively significant, while that from the O′ is weak but definitely present. In contrast, for the ternary alloy, the intensity associated with the O′ reflection is strong relative to weak intensity maxima from the ω phase. It is not immediately clear whether Al additions to the ternary alloy tend to stabilize the O′ phase, or simply de-stabilize the ω phase. To assist in identifying the role of Al additions, a sample of Ti-18Mo-5Al, solution treated and quenched, was subsequently aged isothermally at 300°C for 48hrs. Atom probe tomography was employed to assess the variations in Al and oxygen compositions across the interface between the β phase and an ω particle, and the results are shown in Fig. 2(b-c). A 3D atom probe reconstruction of the needle shape sample ~76 nm long shows the iso-concentration surface for 90% Ti with Al atoms in green and Mo atoms in red, revealing three ellipsoidal morphology ω particles in Fig. 2(b). As can be seen in the proxigram generated from all three ω particles shown in Fig. 2(c), the Al composition is low in the aged ω particle and rises rapidly in the β matrix. In contrast, the oxygen content is more or less at a constantly low value across the interface; some small variations may be present in the vicinity of the interface, but these are hardly statistically significant. When this compositional variation

in Al is taken together with the change in intensity profiles in the SAD patterns, it appears that the role of Al is to destabilize the ω phase. However, its direct effect on the O′ phase is not obvious. This has been solved by comparing the intensities of the diffraction maxima from the O′, with background subtracted, with that of a fundamental reflection from the β phase (not saturated in the diffraction pattern) measured in patterns recorded with the beam parallel to $<100>_{\beta}$. Thus, it is found that from three measurements, in the binary alloy, the ratio of these intensities is 0.0067±0.001 compared with that in the ternary (i.e., Al containing) where a ratio of 0.03±0.005 is measured. From these measurements, it appears that additions of Al do indeed increase the stability of the O′ phase.

The microstructure of as-quenched Ti-18Mo-5Al with yttrium added, where the amount of yttrium is in excess of that required to form the oxide, Y_2O_3, has been characterized. Relatively large particles have formed in the β matrix, Fig. 3(a), and these contain both yttrium and oxygen as revealed by measurements involving STEM XEDS, shown in Fig. 3(b). While it has not been possible to perform accurate quantitative analysis of the oxygen content in the β phase matrix, the presence of such oxygen enriched particles can be treated as evidence, that the oxygen concentration in the β matrix is very significantly reduced from the initial overall content of 0.26wt%. This is consistent with the results of a systematic investigation reported in a previous study where it was determined that the addition of YH_2 into CP Ti and Ti-6Al-4V can help form an essentially oxygen-free β matrix [16]. The question arises whether the excess yttrium is present in a significant amount in the β matrix to perhaps influence the stability of the ω and O′ phases. For this reason, XEDS measurements were recorded from the β matrix and no characteristic peaks from yttrium were observed. Thus, it appears that the Y containing particles may be partially oxidized and Fig. 3(a-b) qualitatively support this suggestion. Additionally, the distribution and size of the yttrium containing particles are heterogeneous and no evidence has been found of such particles having influenced the formation of the uniformly distributed fine-scaled ω phase and the O′ phase. Samples of the quenched alloy Ti-18Mo-5Al+Y were examined using HAADF imaging to show the presence of the O′ phase. Fig. 3(c and d) show such images from the β matrix and the O′ phase, respectively. The presence

of the O′ phase, essentially in the absence of oxygen, is clearly demonstrated. To establish whether the absence of oxygen from the matrix resulted in changes in the stability of either the ω or O′ phase, SAD patterns were recorded with the electron beam parallel to $<110>_{\beta}$, as shown in Fig. 4 (a and b), for the two alloys Ti-18Mo+Y and Ti-18Mo-5Al+Y, and intensity profiles were extracted as in Fig. 2(a). These are shown as insets in the figures. The profiles from both alloys containing yttrium are essentially the same as those obtained for the alloys without yttrium additions. This demonstrates that the absence of oxygen does not prevent the formation of metastable ω and O′ phase.

In our previous study [11], it was suggested that the composition and temperature dependences of structural instabilities in the β phase (i.e., the {111}<112> shear related to the Bain distortion that transforms the β phase to martensite), the $\{110\}<1\bar{1}0>$ transverse wave (i.e., the shuffle which provides the correct stacking of planes in the martensite), and the 2/3<111> longitudinal phonon (that leads to ω) determine which of these metastable phases dominate the quenched microstructure. In this context, the effect of Al and Zr on the stability of martensite in β stabilized alloys is anomalous. Thus, it is known that these elements, which are otherwise an α stabilizer (Al) or a neutral element (Zr), suppress the formation of martensite [17, 18]. Our current results, together with our earlier work [10], demonstrate that Al and Zr additions promote the $\{110\}<1\bar{1}0>$ transverse wave component of the martensitic transformation over the {111}<112> shear, leading to the formation of nanodomains of the O′ phase. This phase cannot be regarded strictly as a martensite, as suggested in [6], since there is no Bain distortion associated with the transformation, but is rather more properly identified as a displacement driven phase transformation. In addition, our results show that both Al and Zr additions destabilise the ω phase. Further, it has been clearly demonstrated in the current research that the formation of nano-scale O′ phase does not require the addition of interstitial oxygen and therefore it appears that O′ phase arises from the intrinsic $\{110\}<1\bar{1}0>$ transverse instability in the β matrix of metastable β titanium alloys. Indeed, the present results suggest that oxygen is not a necessary alloying addition to form the O′ phase in the metastable β titanium alloys, such as Ti-18Mo and Ti-18Mo-5Al alloys.

Acknowledgements

The support of this research by the National Science Foundation, under grant DMR-1309270, is very gratefully acknowledged. One of the authors, DB, acknowledges the grant of the JC Bose Fellowship of the Department of Science and Technology of the Government of India.

References:

[1] D. Banerjee, J.C. Williams, Acta Mater., 61 (2013) 844-879.
[2] Y. Zheng, R.E.A. Williams, D. Wang, R. Shi, S. Nag, P. Kami, J.M. Sosa, R. Banerjee, Y. Wang, H.L. Fraser, Acta Mater., 103 (2016) 850-858.
[3] S.A. Mantri, D. Choudhuri, A. Behra, J.D. Coton, N. Kumar, R. Banerjee, Matel. Mater. Trans. A, 46 (2015) 2803-2808.
[4] T. Yano, Y. Murakami, D. Shindo, S. Kuramoto, Acta Mater., 57 (2009) 628-633.
[5] M. Tahara, H.Y. Kim, T. Inamura, H. Hosoda, S. Miyazaki, Acta Mater., 59 (2011) 6208-6218.
[6] Y. Wang, J. Gao, H. Wu, S. Yang, X. Ding, D. Wang, X. Ren, Y. Wang, X. Song, J. Gao, Sci. Rep., 4 (2014).
[7] D. Wang, Y. Wang, Z. Zhang, X. Ren, Phys. Rev. Lett., 105 (2010) 205702.
[8] D. Wang, Z. Zhang, J. Zhang, Y. Zhou, Y. Wang, X. Ding, Y. Wang, X. Ren, Acta Mater., 58 (2010) 6206-6215.
[9] D. Banerjee, K. Muraleedharan, J.L. Strudel, Phi. Mag. A, 77 (1998) 299-323.
[10] Y. Zheng, R.E.A. Williams, S. Nag, R. Banerjee, H.L. Fraser, D. Banerjee, Scr. Mater., 116 (2016) 49-52.
[11] Y. Zheng, D. Banerjee, H.L. Fraser, Scr. Mater., 116 (2016) 131-134.
[12] W.G. Burgers, Physica., 1 (1934) 561-586.
[13] D. Banerjee, A.K. Gogia, T.K. Nandi, V.A. Joshi, Acta Metall., 36 (1988) 871-882.
[14] Y. Zheng, R.E.A. Williams, H.L. Fraser, Scr. Mater., 113 (2016) 202-205.
[15] D.G. Konitzer, J.P.A. Lofvander, S.A. Court, R. Kirchheim, H.L. Fraser, Acta Metall., 36 (1988) 1595-1606.
[16] M. Yan, Y. Liu, G.B. Schaffer, M. Qian, Scr. Mater., 68 (2013) 63-66.
[17] J.C. Williams, B.S. Hickman, D.H. Leslie, Met. Tran., 2 (1971) 477-484.
[18] M. Abdel-Hady, K. Hinoshita, M. Morinaga, Scr. Mater., 55 (2006) 477-480.

Figure Captions:

Fig. 1. The O′ phase in Ti-18Mo-5Al. (a) SAD pattern with the electron beam parallel to $<110>_{\beta}$ showing reflections consistent with the ω and O′ phases. (b) Dark-field TEM micrograph formed using the diffracted intensity from the O′ phase (white circle) shown in

the <100>$_\beta$ SAD pattern (inset). c) and d) HAADF images showing the O′ and ω phases, respectively, in as-quenched Ti-18Mo-5Al.

Fig. 2. (a) The intensity profiles from SAD patterns plotted along the dashed white line in Fig. 1(a) showing the relative intensities of the ω and O′ diffracted intensities in Ti-18Mo-5Al (blue) and Ti-18Mo (red). (b) 3D atom probe reconstruction of needle shaped sample represented by 90% Ti iso-concentration surface with Al atom (green color spot) and Mo atom (red color spot). (c) Compositional determinations using atom probe tomography showing the partitioning of Al and oxygen between the ω and β phases in Ti-18Mo-5Al isothermally aged at 300°C for 48hrs; these data are the averages of the composition profiles obtained from each of the three ω particles imaged in Fig. 2(b).

Fig. 3. (a and b) XEDS maps of yttrium oxide particles in the Ti-18Mo-5Al+Y alloy. (c and d) HAADF images showing the β and O′ phases in the same alloy, with intensity profiles plotted along the direction of the dashed white lines.

Fig. 4. (a and b) Selected area diffraction patterns recorded with the electron beam parallel to <110>$_\beta$ for Ti-18Mo+Y and Ti-18Mo-5Al+Y, respectively. The presence of the O′ phase is confirmed in both alloys. The insets are intensity profiles plotted along the dashed white lines in each case.w

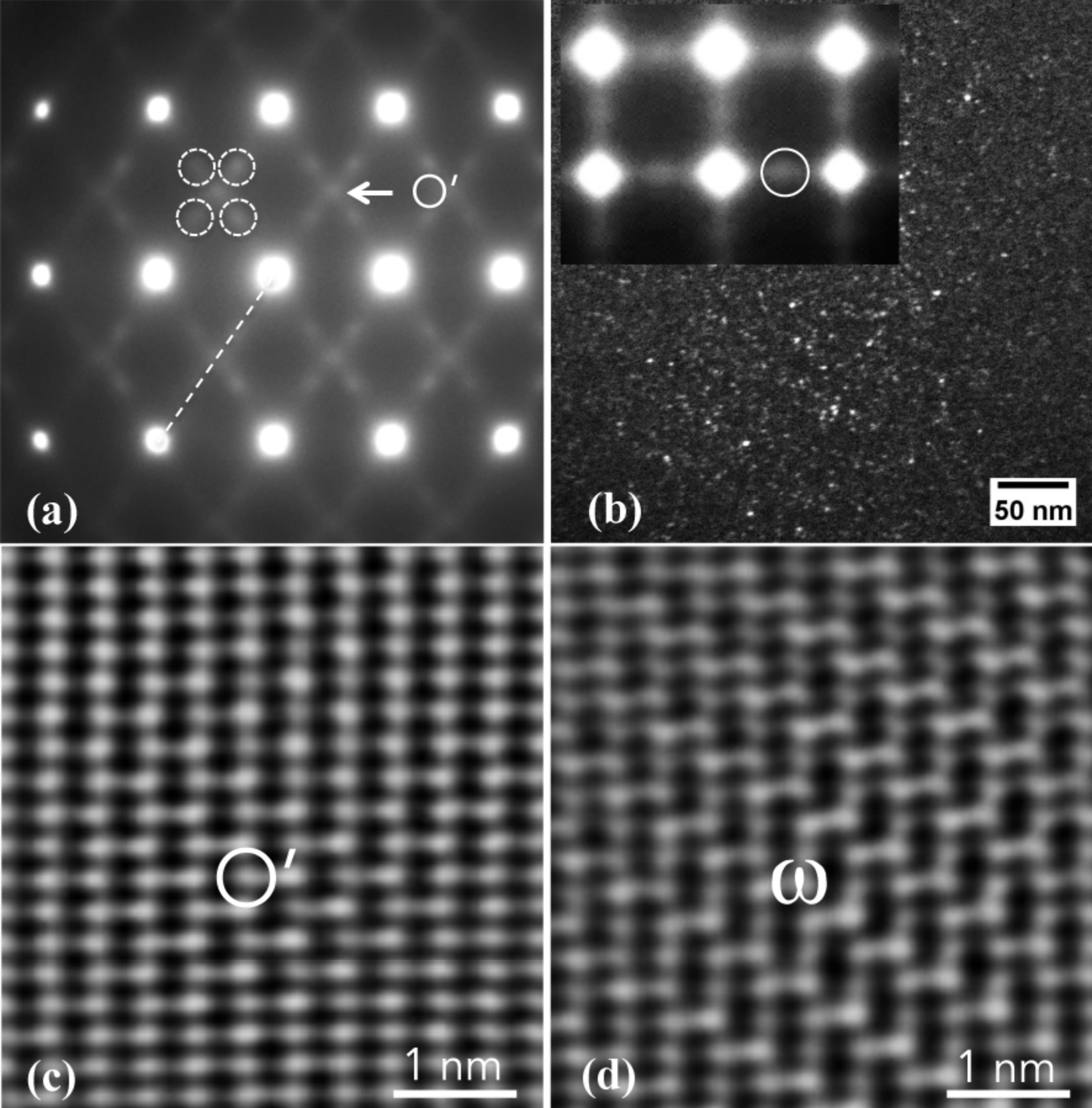
O′
(a)
(b)
50 nm
O′
1 nm
(c)
ω
1 nm
(d)

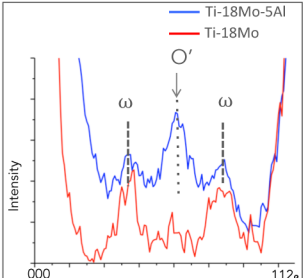
Ti-18Mo-5Al
Ti-18Mo
O′
ω
ω
Intensity
000
112β

(a)

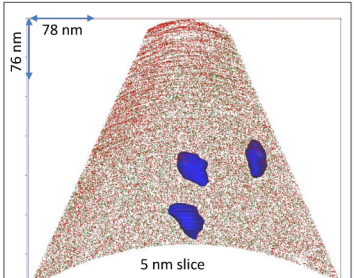
78 nm
76 nm
5 nm slice

(b)

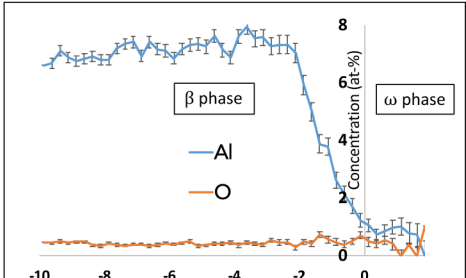
β phase
ω phase
Al
O
Concentration (at-%)
Distance (nm)
8
6
4
2
0
-10
-8
-6
-4
-2
0

(c)

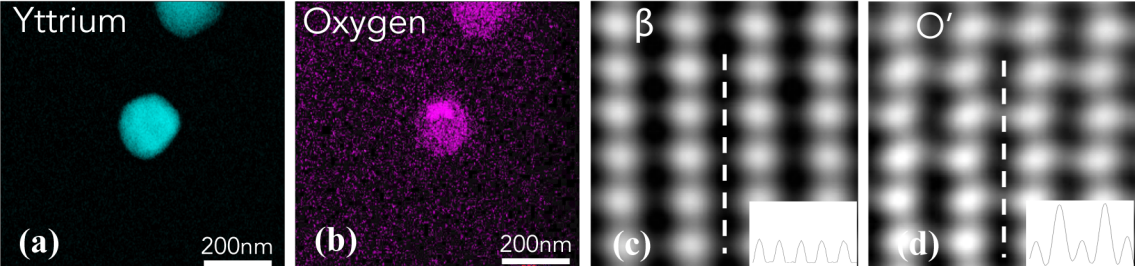
Yttrium
(a)
200nm
Oxygen
(b)
200nm
β
(c)
O′
(d)

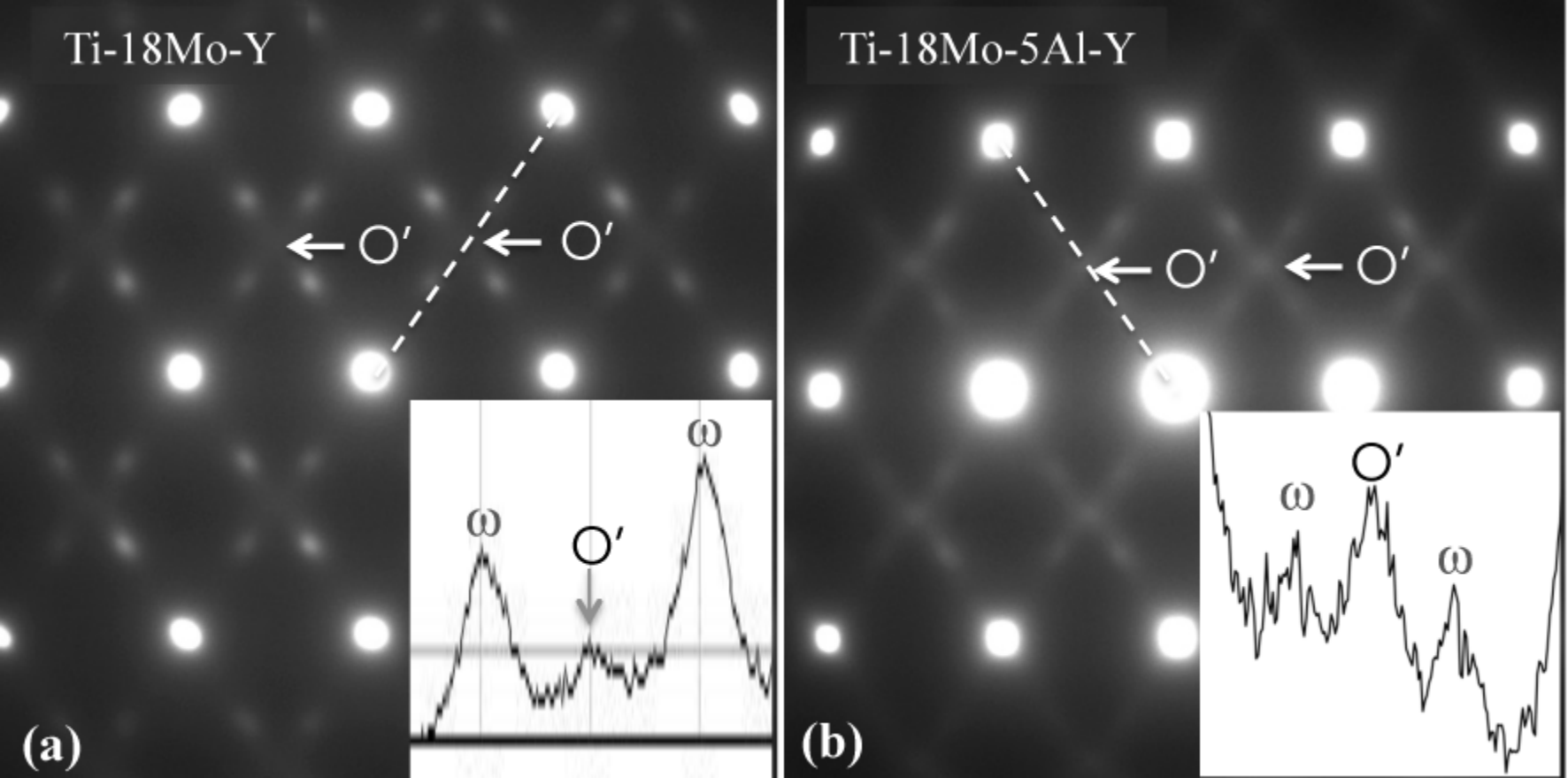
Ti-18Mo-Y
O′
O′
ω
ω
O′
(a)
Ti-18Mo-5Al-Y
O′
O′
ω
O′
ω
(b)

Ti-18Mo-5Al+Y